Tribological behaviors in air and seawater of CrN/TiN superlattice coatings irradiated by high-intensity pulsed ion beam

5 authors, including:

Yixiang Ou
Beijing Normal University

23 PUBLICATIONS   **229** CITATIONS

Some of the authors of this publication are also working on these related projects:

Project   HiPIMS tribological coatings View project

Project   Effects of nanoscale interfaces on ionic conductivity in superlatticed thin films View project
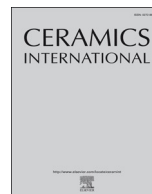
Tribological behaviors in air and seawater of CrN/TiN superlattice coatings irradiated by high-intensity pulsed ion beam

Y.X. Ou[a,b,*], H.Q. Wang[b], B. Liao[b], M.K. Lei[c], X.P. Ouyang[d]

[a] Beijing Radiation Center, Beijing Academy of Science and Technology, Beijing, 100875, China
[b] Key Laboratory of Beam Technology and Material Modification of Ministry of Education, College of Nuclear Science and Technology, Beijing Normal University, Beijing, 100875, China
[c] Surface Engineering Laboratory, School of Materials Science and Engineering, Dalian University of Technology, Dalian, 116024, China
[d] Northwest Nuclear Technology Institute, Xi'An, 710024, China

A B S T R A C T

Surface integrity and interface structure of coating materials play a key role in tribological and corrosion behaviors in harsh working environments in nuclear power plants. In this work, we focus on the investigations of tribological behaviors in air and seawater of CrN/TiN superlattice coatings deposited by the combined deep oscillation magnetron sputtering with pulsed dc magnetron sputtering, which were irradiated by high-intensity pulsed ion beam (HIPIB) with ion energy density of 1–3 J/cm^2 and shot number of 1–5. At 1 J/cm^2, the increased shot number leads to a broaden (111) peak of face-centered cubic crystal structure, indicating grain size refinement. At 3 J/cm^2, the increased shot number results in the coarsening grain, and superlattice structure gradually disappeared at 2 shots, finally the coatings fell off from substrate at 5 shots. The highest hardness (H), H/E* (E*, effective Young's modulus) and H^3/E*^{2} of the coatings irradiated at 1 J/cm^2 and 5 shots are achieved at 38.7 GPa, 0.1 and 0.387, respectively. The increased ion energy density and shot number result in the decrease in Rockwell C HF adhesion level from HF1 to HF6. At 1 Jcm^{-2} and 1 shot, tribological behavior of irradiated coatings in air was dominated by oxidative wear with coefficient of friction (COF) of 0.51 and specific wear rate of 4.2×10^{-7}mm^{3}N^{-1}m^{-1}. The irradiated coatings show excellent tribocorrosion properties in seawater with high open circuit potential of 0.32 V, low COF of 0.14 and specific tribocorrosion rate of 6.1×10^{-8}mm^{3}N^{-1}m^{-1} without pitting corrosion under moderate HIPIB irradiation due to high surface integrity and stability of well-defined interfaces and dense microstructure. With an increase of energy density and shot number, wear mechanism in air changes to severe adhesive and oxidative wear, while tribocorrosion mechanism is gradually dominated by plough wear coupled with pitting corrosion.

1. Introduction

Austenitic stainless steels have been widely used to fabricate mechanical components, such as pumps and valves in nuclear power plants due to their good corrosion resistance, weldability and fabricability. However, poor friction and wear properties of austenitic stainless steels have been a barrier against their applications in harsh working environment in terms of wear, corrosion and radiation. Hence, various surface modification techniques have been developed to enhance working performance, reliability and durability of austenitic stainless steels. Among them, surface nitriding processes, including gas, plasma and laser nitriding, are extensively applied to improve wear resistance of austenitic stainless steels [1–4]. The combined improvement in wear and corrosion resistance would be obtained by the precise control of

nitriding temperature to avoid chromium nitride precipitation above 400 °C [5]. Besides, plasma nitriding process always consumes a long time (at less 4 h), beneficial for the nitrogen diffusion in austenitic stainless steels to form brittle nitride layers with only several micrometers thickness.

Advanced coatings deposited on austenitic stainless steels can produce the coated surface with the combined improvement of wear and corrosion resistance. As compared with surface nitriding processes, preparation techniques have distinct advantages to tailor composition, structure and properties at a high deposition rate [6,7]. However, it is noted that conventional magnetron sputtering process always results in porous microstructure owing to low ionization density of target species [8], while vacuum arc processes are hard to eliminate the formation of micro-particles and porosity in coatings [9,10]. High-power pulsed

magnetron sputtering (HPPMS)/high power impulse magnetron sputtering (HiPIMS) and modulated pulsed power magnetron sputtering (MPPMS) can generate highly ionized target species with high density by applying a series of pulsed-power to target in a short period of time [11–14].

As a novel high-power pulse technique, deep oscillation magnetron sputtering (DOMS) is a flexible and efficient process to produce high-performance coatings [15]. As compared with HPPMS/HiPIMS and MPPMS, DOMS can achieve high ionization degree and plasma density in reactive sputtering under optimized conditions. TiAlSiN nano-composite coatings [7] or CrN/TiN superlattice coatings [16,17] deposited on austenitic stainless steels by DOMS at room temperature exhibit high hardness, toughness and adhesion, along with excellent wear and corrosion resistance. In addition, it is reported that TiN-based coatings can be used as the inert matrixes proposed to surround the fuel in future gas cooled fast reactor systems. Ti–Zr–N [18] and (TiHfZrNbVTa)N coatings [19] show good stability of microstructure and properties under high Xe-ion irradiation and negative heavy-ion implantation of Au^{-1}, respectively, indicating a promising perspective in nuclear industrial application. Nevertheless, there are limited studies on wear and corrosion resistance, especially for tribocorrosion behavior of CrN/TiN superlattice coatings after irradiation. Therefore, it is essential to investigate tribological behaviors of CrN/TiN superlattice coatings deposited by DOMS to explore the influence of irradiation dose on dry friction in air and tribocorrosion behaviors in seawater.

Tribocorrosion is a complex tribological behavior in corrosive medium coupled simultaneous action of wear and corrosion, resulting in a material deterioration or transformation [20,21]. When the coated surface is subjected to tribo-corrosion contacts, tribocorrosion behavior of hard coatings is influenced by surface morphology, composition, microstructure, residual stress state and cohesion/adhesion [22]. Chen et al. [23] showed that CrN coatings greatly enhanced tribocorrosion behaviors of austenitic stainless steels in 3.5 wt% NaCl aqueous solution, but lots of micro-cracks caused by friction forces acted as diffusion channels for Cl ion to result in intersecting cracks and coating delamination. Shan et al. [24] reported dominated wear behavior PVD CrN coated stainless steel in seawater gradually changed from mechanical wear (plastic deformation) to corrosion-accelerated wear, resulting in pitting corrosion in wear tracks with increasing anodic potentials. Monticelli et al. [25] presented comparative studies of corrosion and tribocorrosion behaviours of cermet and cermet/nanoscale multilayer CrN/NbN coatings in 3.5% NaCl solutions. The duplex nanoscale multilayer CrN/NbN/WC-12Co coatings exhibited excellent corrosion resistance both corrosion and tribocorrosion resistance. Thus, high surface integrity and dense interface structure are expected to significantly enhance tribocorrosion properties in aggressive solutions.

High intensity pulsed ion beam (HIPIB) has been widely used for thin-film depositions, surface modification and ion implantation in semiconductors [26–29]. That is because HIPIB ion beams with relatively low power density of $10^6–10^9 \, W/cm^2$ are very promising for industrial applications. In this work, CrN/TiN superlattice coatings with modulated period (Λ) of 6.3 nm were deposited on AISI 304L stainless steel substrates by the combined DOMS with pulsed dc magnetron sputtering. And then, the coatings irradiated at 1–3 J/cm^2 and 1–5 shots using HIPIB were investigated to explore correlations of the evolution of structure, adhesion and mechanical properties with tribological behaviors in air and seawater and corresponded mechanisms of the irradiated coatings.

2. Experimental details

About 3 µm thick CrN/TiN superlattice coatings (Λ = 6.3 nm) were deposited on AISI 304L austenitic stainless steels (15 mm × 15 mm × 2 mm) using the combined deep oscillation magnetron sputtering (DOMS) and pulsed dc magnetron sputtering (PDCMS) at room temperature. Cr and Ti targets were powered by

Table 1
Typical HIPIB parameters used to irradiate CrN/TiN superlattice coatings deposited by DOMS + PDCMS.

Ion species	70% proton and 30% carbon ions
Ion accelerating voltage	220 kV
Ion current density	200A/cm^2
Pulse width	70 ns
Shot number	1–5
Power density	~$10^8 \, W/cm^2$
Energy density	1–3 J/cm^2

DOMS power supply (HIPIMS Cyprium™ plasma generator, Zpulser, LLC) at 400W and PDCMS power supply (Pinnacle Plus, Advance Energy) at 2000W with 100 kHz and 90% duty cycle, respectively. More information about DOMS pulse shape, deposition conditions and properties of the as-deposited coatings can be found in Rf [16]. As-deposited coatings were irradiated at ion energy density of 1–3 J/cm^2 and shot number of 1–5 at 220 kV using a TEMP high-intensity unipolar-mode pulsed ion source consisting of pulsed power systems and ion diode systems [27]. Typical HIPIB parameters used to irradiate CrN/TiN superlattice coatings deposited by DOMS + PDCMS are shown in Table 1.

The crystallographic structure of HIPIB-irradiated coatings was detected using Siemens KRISTALLOFLEX-810 type X-ray diffraction (XRD) in θ-2θ configuration with the Cu Kα radiation. The microstructure feature of the HIPIB-irradiated coatings was investigated using both ZEISS SUPRA-55 VP type field emission scanning electron microscope (FESEM) and Philips/FEI CM200 type transmission electron microscope (TEM). Surface roughness of the coatings after HIPIB irradiation was measured by Taylor Hobson surface profilometer. The adhesion of HIPIB-irradiated coating was evaluated using standard Rockwell C hardness tests. Adhesion level of HIPIB-irradiated coatings was determined according to FESEM morphology feature of indentations. Tribological behaviors in air and seawater (3.5 wt% NaCl aqueous solution) were investigated using MFT-EC4000 type reciprocating tribometer. Dry sliding wear tests of the irradiated coatings were carried out under a normal load of 5 N and 1 Hz at room temperature for the sliding time of 30 min against AISI 306L stainless steel balls (Φ6 mm). Tribocorrosion tests were performed at a tailored electrolyzer integrated with a three-electrode electrochemical system. The change of open circuit potential (OCP) with the sliding time were studied under constant current mode. The normal load of 5 N and reciprocating frequency of 1 Hz at room temperature was applied during the tests against Si$_3$N$_4$ counterpart balls. The reciprocating length was fixed at 5 mm during tests in air and seawater. Specific wear rate was calculated according to wear track profile, which was analyzed using Taylor Hobson surface profilometer. Tribocorrosion samples was cleaned by deionized water for calculation specific tribocorrosion rate. Worn surface morphologies were observed using FESEM and an optical microscope further studying wear and tribocorrosion mechanisms.

3. Results

3.1. Structure

Fig. 1 shows the XRD spectra and FESEM morphologies of HIPIB-irradiated CrN/TiN superlattice coatings deposited on AISI 304L austenitic stainless steels by the combined DOMS + PDCMS. As shown in Fig. 1a, strong (111) and weak (222) peaks from face-centered cubic (*fcc*) crystal structure are observed in XRD diffraction patterns of HIPIB-irradiated coatings at energy density of 1 Jcm^{-2} with shot number of 1–5, besides diffraction peaks of 304L austenitic stainless steels substrates (labeled as SS) and Cr adhesion layers. In addition, no broadening and shifting of peaks are detected in the patterns. Thus, it reveals that (111)-textured coatings still exhibit high structure stability without
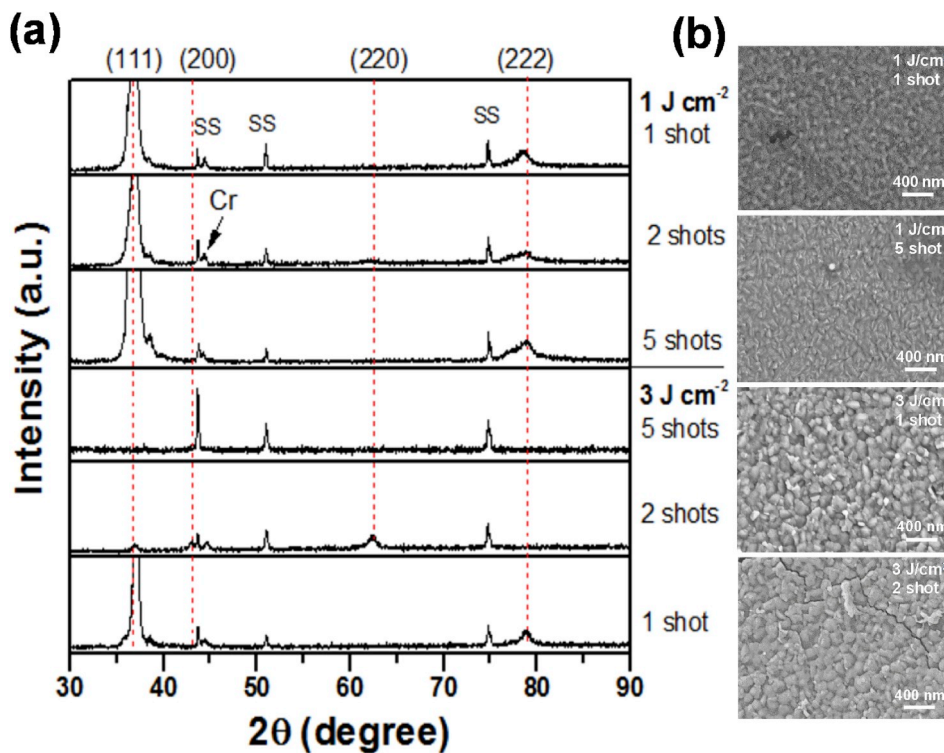
Fig. 1. (a) XRD spectra and (b) FESEM morphologies of HIPIB-irradiated CrN/TiN superlattice coatings deposited on AISI 304L austenitic stainless steels by the combined DOMS + PDCMS.

the disappearance of superlattice structure, compared with that of as-deposited coatings [16]. Nevertheless, (111) diffraction peak of HIPIB-irradiated coatings at 3 Jcm^{-2} and 1 shot shows a slight shifting to a higher diffraction angle along with the decrease of peak width, probably indicting the grain coarsening and increased residual stress. Meanwhile, the irradiated coatings still have a stable superlattice structure because satellite peaks around the strong (111) main peak are clearly observed [17]. When the coatings are irradiated at 3 Jcm^{-2} and 2 shots, the intensity of (111) peak from *fcc* structure sharply decreased, as well as the disappearance of (222) peak and satellite peaks. The (111) peak shifted from 36.78° at 1 Jcm^{-2} to a higher angle of 37.09°. Meanwhile, weak (200) and (220) peaks are detected in spectra. Further increasing shot time to 3, only peaks from 304L substrate are observed because the coatings already fell off substrate. It is well known that the orientation of coating growth depends on the competitive relationship between surface energy ($S_{200}^< S_{220}^< S_{111}$) and strain energy ($U_{200} > U_{220} > U_{111}$) [30,31]. It is reported that DOMS plasma with high density and ion flux is prone to promote (111) preferred orientation, which is benefited from the enhanced ability of adatom mobility at surface caused by appropriate ion bombardment [8,17]. Hence, in this case, (111)-textured DOMS coatings under HIPIB strong ion impact show a random orientation feature owing to the achievement of the balance of surface energy and strain energy.

Fig. 1b presents FESEM morphologies of HIPIB-irradiated CrN/TiN superlattice coatings deposited on AISI 304L austenitic stainless steels by the combined DOMS + PDCMS. The irradiated coatings at 1 Jcm^{-2} and 1–5 shots exhibit smooth and dense morphologies without any changes of surface feature due to high structural stability, agreed with XRD results. The measured surface roughness (R_a) is in the range of 17–26 nm. The grain size is about 38 nm. When the coatings are irradiated at 3 Jcm^{-2} and 1 shot, and grain size increased to about 122 nm consist with broadening XRD diffraction peak. However, at 3 Jcm^{-2} and 2 shots, high energy density and irradiated time promote the increased grain size and R_a up to 200 nm and 48 nm, respectively. The river-like fine cracks along grain boundaries are clearly observed on

HIPIB-irradiated surface, which is probably resulted from grain coarsening and stress-relaxed at grain boundaries caused by thermal-dynamic effects of HIPIB [32]. It is also found that microcracks along boundary were observed in Cr$_2$O$_3$ coatings irradiated by HIPIB due to the effects of rapid melting and accordingly fast solidification on the ablated surface [33].

Fig. 2 presents the cross-sectional TEM image, high resolution TEM micrograph with selected area electron diffraction (SAED) patterns inserted of the HIPIB-irradiated coatings at 1 Jcm^{-2} and 1 shot. As compared with TEM morphologies of as-deposited coatings [16], it is clearly seen that the irradiated coatings still keep dense interfaces (coating/substrate and Cr adhesion/coatings) in Fig. 2a, well-defined CrN/TiN nanolayers interfaces and dense grain boundaries in Fig. 2b. Dense microstructure features well agreed with XRD and FESEM results. The SAED patterns show distinct diffraction rings assigned to (111), (200) and (220) reflections from *fcc* crystal structure of irradiated CrN/TiN superlattice coatings.

3.2. Hardness and Young's modulus

Hardness (H) and Young's modulus (E) of HIPIB-irradiated coatings deposited on AISI 304L stainless steel by the combined DOMS + PDCMS are showed in Table 2. H/E* and H^3/E*^{2} ratios are calculated using H and effective Young's modulus (E*, E* = E/(1-v^2), where v is Poisson's ratio. At 1 Jcm^{-2}, a slight increase of H and E from 36.4 and 375 to 38.7 GPa and 389 GPa, respectively, is observed with increasing shot number from 1 to 5. H/E* and H^3/E*^{2} ratios are correspondingly increased from 0.097 and 0.343 to 0.1 and 0.387, respectively. According to XRD results, there are no observations for transition of crystal structure, phase composition and grain size contributed for the increased H and E of HIPIB-irradiated coatings. As for HIPIB technique, it is novel shock processing to induce high-density defects with residual compressive stresses in controlled depth into sample surface using shock wave propagation [20]. Thus, the slight enhancement in H and E may be related to the residual stress state.
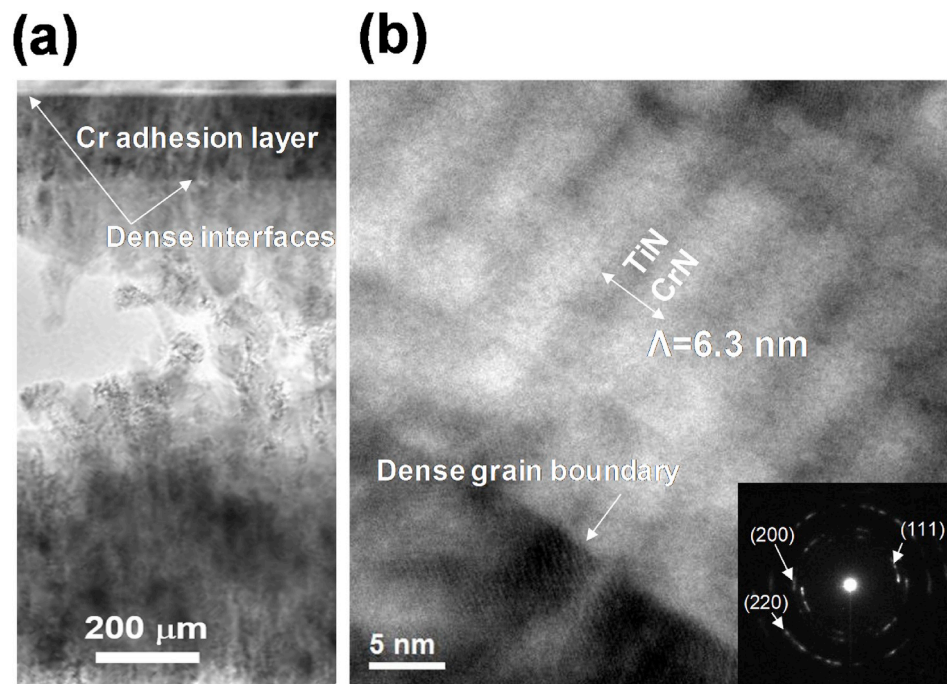
Fig. 2. (a) Cross-sectional TEM image and (b) high resolution TEM micrograph with selected area electron diffraction (SAED) patterns inserted of the HIPIB-irradiated coatings at 1 Jcm^{-2} and 1 shot.

When energy density is 3 Jcm^{-2}, obvious decrease in H, E, H/E*, H^3/E*^{2}–26.3 GPa, 288 GPa, 0.092 and 0.219, respectively, with an increase in shot number from 1 to 2 as a result of grain coarsening according to Hall-Patch effect [34]. In addition, the formation of microcracks along grain boundaries may contribute for the decrease of mechanical properties due to stress release [32,33].

3.3. Adhesion

The adhesion strength of HIPIB-irradiated coatings deposited on AISI 304L stainless steel by the combined DOMS + PDCMS is assessed by Rockwell C indentations [35]. That is because the soft substrate can produce a large amount of plastic deformation under the standard load [31,36]. Fig. 3 shows Rockwell C indentations and adhesion level (HF) of HIPIB-irradiated coatings at 1–3 Jcm^{-2} and 1–5 shots. As shown in Fig. 3a-c, the coatings irradiated at 1 Jcm^{-2} by HIPIB exhibit good adhesion to substrate (HF1), thanks to high stability of crystal structure and mechanical properties. At 3 Jcm^{-2}, radial cracks and the edge of delamination of indentations are clearly seen when shot number of 1–2 (Fig. 3d and e). When the coating was shot at 5 times, the coatings almost fell off (Fig. 3f). Thus, the adhesion of CrN/TiN superlattice coatings deposited by the combined DOMS + PDCMS can sustain the HIPIB impact of high energy density at 3 Jcm^{-2} and 2 shots.

3.4. Tribological behaviors in air

Tribological behaviors in air of HIPIB-irradiated CrN/TiN superlattice coatings at energy density of 1–3 Jcm^{-2} and shot number of 1–5 was investigated using dry sliding tests in a reciprocating mode against the same counterpart of 304L stainless steel balls. The normal load of 5 N and reciprocating frequency of 1 Hz were used during wear tests for a sliding time of 30 min. Fig. 4 plots the coefficient of friction (COF) for HIPIB-irradiated CrN/TiN superlattice coatings as a function of sliding time. At 1 Jcm^{-2} and 1 shot, the COF of irradiated coatings presents a sharp increase to 0.51 in 2 min (running-in period), and then exhibits a stable and smooth trend. With an increase in shot number, the COF gradually increases to 0.62, as well as the observation of rough and wave feature. When the energy density increases to 3 Jcm^{-2}, COF of HIPIB-irradiated coatings continue to increase to 0.79 at 2 shots. Besides, COF has a fluctuating tendency during long running-in period time of 12 min, as well as the obvious oscillation feature in stable wear period. The COF of HIPIB-irradiated coatings at 5 shots shows a high value of 0.82 with a strong oscillation feature due to the sliding wear against the exposed substrate surface.

The worn surface of HIPIB-irradiated CrN/TiN superlattice coatings at an energy density of 1–3 Jcm^{-2} and a shot number of 1–5 are inserted in Fig. 4. At 1 Jcm^{-2} and 1 shot, it is clearly seen that worn surface shows smooth morphology covered with thin oxide films. Only shallow grooves and a few wear debris are adhered within wear track. Thus, it is inferred that wear mechanism is dominated by mild oxidative wear. With an increase in shot number, the number of grooves on worn surface increases, but there is no observation for coating failure. The wear mechanism changes from mild oxidative wear to oxidative wear. At 3 Jcm^{-2}, however, the HIPIB-irradiated coatings suffered from

Table 2
Mechanical and tribological properties in air and seawater of CrN/TiN superlattice coatings irradiated by HIPIB.

Dose [J/cm^{-2}]	Shot	H [GPa]	E [GPa]	H/E*	H^3/E*^{2}	COF	Wear rate in air [$\times 10^{-7}$mm^{3}N^{-1}m^{-1}]	Wear rate in seawater [$\times 10^{-7}$mm^{3}N^{-1}m^{-1}]
1	1	36.4	375	0.097	0.343	0.52	4.2	0.61
1	2	37.2	382	0.098	0.353	0.55	8.4	3.7
1	5	38.7	389	0.1	0.387	0.63	10.3	7.8
3	1	35.2	371	0.095	0.317	0.66	13.5	15.1
3	2	26.3	288	0.092	0.219	0.78	14.8	16.8
3	5	3.1	196	–	–	0.82	17.8	–
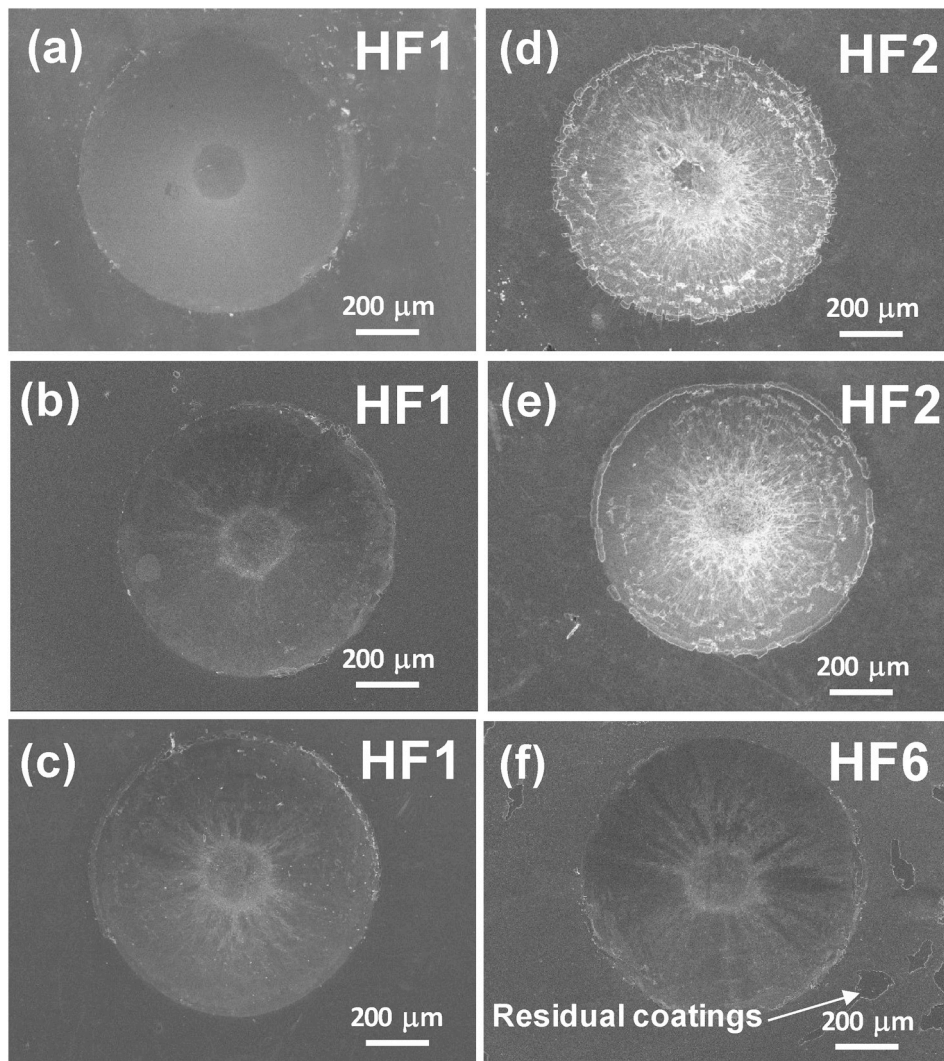
Fig. 3. Rockwell C indentations and adhesion level (HF) of HIPIB-irradiated coatings at 1–3 Jcm^{-2} and 1–5 shots.
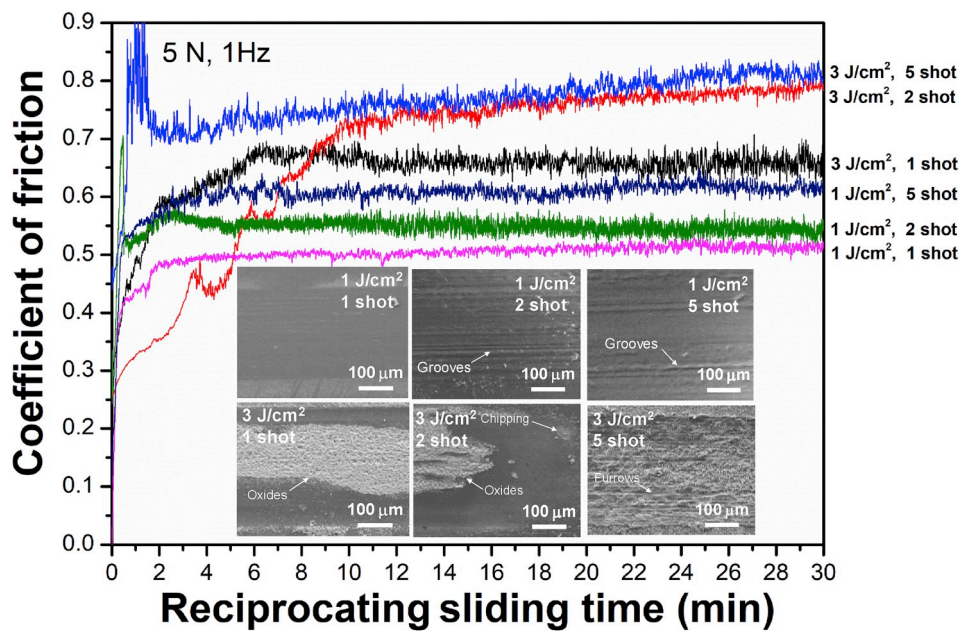
Fig. 4. Coefficient of friction for HIPIB-irradiated CrN/TiN superlattice coatings as a function of sliding time.
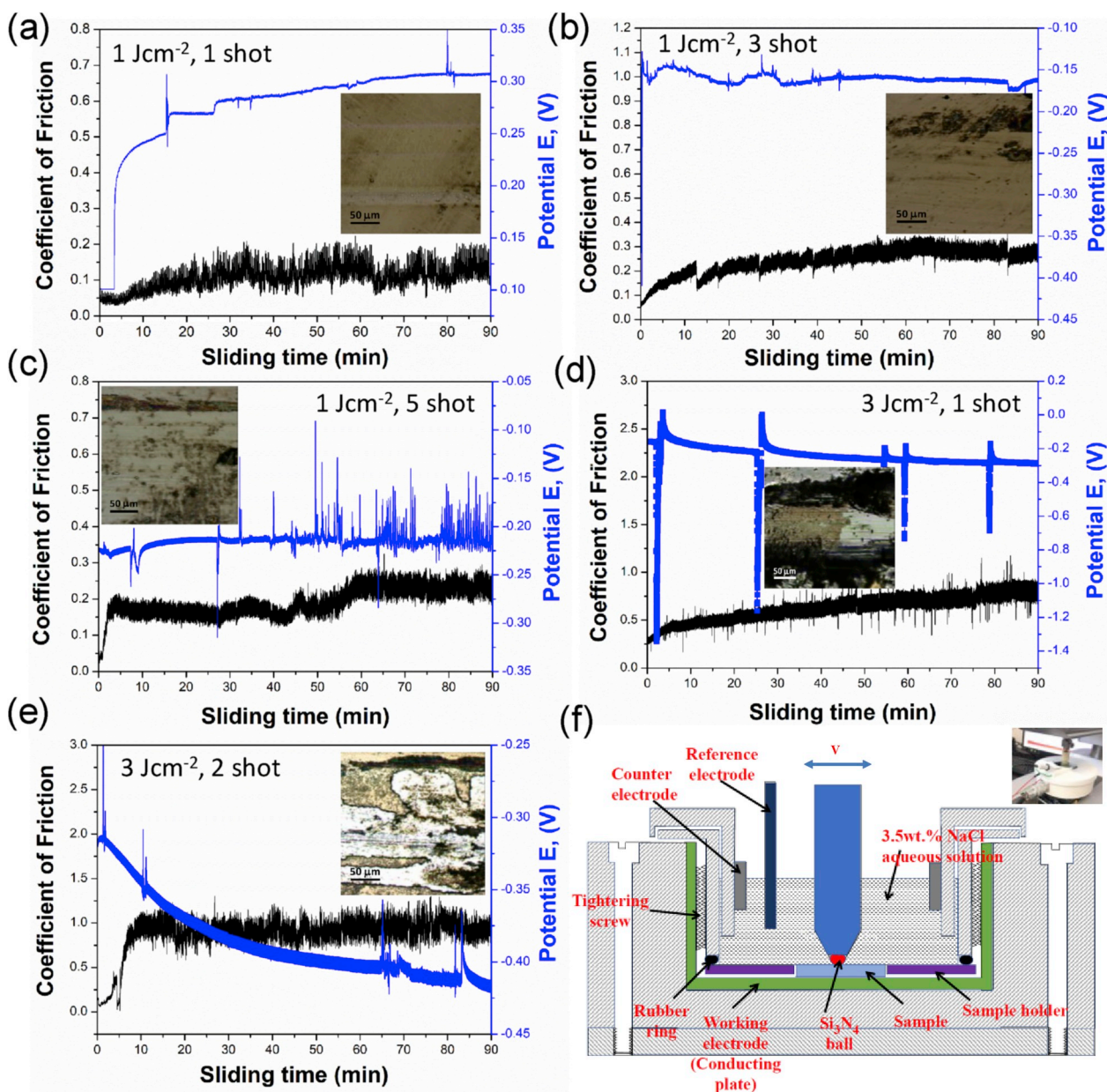
Fig. 5. The changes of OCP and COF as a function of sliding times and the inserted optical micrographs of tribocorrosion tracks for coatings irradiated at an energy density of 1–3 Jcm^{-2} and a shot number of 1–5.

severe oxidation wear with the formation of a large amount of oxides on worn surface. Meanwhile, wear debris was accumulated along both sides of wear track. It is noted that the HIPIB-irradiated coatings at 3 Jcm^{-2} and 2 shots began to chip during dry sliding wear test. When the coatings were shot at 5 times, it already peeled off. Thus, the wear behavior of HIPIB-irradiated coatings at 5 shot belong to the exposed AISI 304L substrate sliding against AISI 304L counterpart balls. The large amount of short furrows and wear debris on worn surface are clearly seen due to the occurrence of severe plastic deformation. The measured specific wear rate ranges from 4.2 to 17.8 × $10^{-7}mm^3N^{-1}m^{-1}$, as shown in Table 2.

3.5. Tribocorrosion behaviors in seawater

Tribological behaviors in seawater is a typical tribocorrosion process, simultaneously coupled with wear and corrosion behaviors. The real-time changes of open circuit potential (OCP) during tribocorrosion solicitations directly reveals in situ electrochemical status of the

electrode surface under tribocorrosion contacts [23,34]. Thus, a qualitative description of electrochemical reactivity is obtained. Fig. 5 exhibits the changes of OCP and COF as a function of sliding times and the inserted optical micrographs of tribocorrosion tracks for coatings irradiated at an energy density of 1–3 Jcm^{-2} and a shot number of 1–5. At 1 Jcm^{-2} and 1 shot, the COF of irradiated coatings shows an oscillation trend, and the average COF is about 0.14. Correspondingly, OCP presents a sharp increase from 0 to 0.25 V, followed by a slight increase to 0.32 V, indicating that the high quality of passive film continuously formed during sliding tests in seawater. Meanwhile, OCP shows relatively stable trend after 15 min, except several pulsating OCP. Surface of tribocorrosion tracks presents smooth morphology along with shallow furrows caused by mild abrasive wear. No visible microcracks and pitting corrosion are observed. Thus, the irradiated coatings at 1 Jcm^{-2} and 1 shot show excellent tribocorrosion resistance in seawater. With increasing shot number, OCP gradually decreases and COF increase due to aggravations of the coupled abrasive wear and pitting corrosion leading to the destruction of dynamic formation of passive

film during tribocorrosion tests, as shown in Fig. 5b and c. In addition, the oscillation trend of OCP, especially in Fig. 5c, reveals the process of breakdown and repairing. The OCP of −0.22 V and COF of 0.25 are obtained at 1 Jcm^{-2} and 5 shots.

At 3 Jcm^{-2} and 1 shot, the OCP of −0.2 V is obtained, while there are four times of sudden decrease of OCP, probably indicating the failure of the irradiated coatings. Tribocorrosion surface shows deep furrows and black debris covered both sides tracks resulted from severe plough wear and pitting corrosion. Noted that the occurrence of pitting corrosion accelerated the wear of irradiated coatings. When shot number is increased to 2, the sharp decrease of OCP to −0.42 V and increase of COF to 1.1 are observed. Massive failure event occurred. And then, visible pittings and furrows are formed on tribocorrosion surface (Fig. 5e). Fig. 5f presents the structure diagram of electrolytic cells used for tribocorrosion tests. The measured specific wear rate ranges from 0.61 to 16.8 × 10^{-7}mm^{3}N^{-1}m^{-1}, as shown in Table 2.

4. Discussion

It is well demonstrated that CrN/TiN superlattice coatings with Λ of 6.3 nm deposited on AISI 304L austenitic stainless steels by the combined DOMS + PDCMS exhibits excellent hardness, toughness, wear and corrosion resistance [16,17]. Aim at the issues of wear and wear, corrosion and radiation of coated components in nuclear power plants, combining practical and research experiences of CrN/TiN superlattice coatings, we focus on the investigations of tribological behaviors in air and seawater of the HIPIB-irradiated CrN/TiN superlattice coatings with Λ of 6.3 nm. At 1 J/cm^2 and 1–5 shots, the coatings still show stable superlattice structure with a strong (111) texture and smooth surface morphology, attributable to the low energy density delivered and the insufficient accumulation of energy to produce renucleation and coarsening of the grain. A slight peak shifting to a higher angle (at 5 shots) probably results from the introduce of residual compressive stresses in coatings. Accordingly, the slight increase in hardness, H/E* and H^3/E^{*2} is observed with increasing shot number. It is revealed that the increased residual stress contributes for XRD peak shift and hardness enhancement [37,38]. Moreover, the coatings still have high adhesion (HF1) without interfacial failure.

At 1 J/cm^2 and 1 shot, the irradiated CrN/TiN superlattice coatings show excellent tribological properties in air and tribocorrosion properties in seawater owing to high stability of well-defined interface and dense microstructure. Wear mechanism in air of HIPIB-irradiated coatings changes from mild oxidative wear to oxidative wear with increasing COF and wear rate due to the increased residual compressive stresses induced by increasing shot number. In addition, the occurrence of pitting corrosion of irradiated coatings with increased defects and residual stress led to tribocorrosion in terms of plough and abrasion wear. Meanwhile, the continuous formation of passive thin films was destroyed due to severe tribocorrosion, resulting in sharply decrease of OCP and increase of COF and specific tribocorrosion rate. In initial period of tribocorrosion of CrN coatings in seawater [24], friction and wear are dominated by plastic deformation, and then severe wear was accelerated by the occurrence of pitting corrosion with increasing OCP during sliding wear tests. At the same time, as for the typical columnar structure of CrN coatings, micro-cracks would be easy to induce by frictional forces to act as diffusion channels for Cl ion, ultimately resulting in degradation of the coatings [23]. Multilayer coatings, such as Cr/GLC coatings [22], CrN/NbN coatings [25], are proved to be good strategies to improve tribocorrosion properties in seawater thanks to the increase of interfaces acted as a strong barrier for Cl ions diffusion.

With an increase in energy density and shot number of HIPIB irradiation, the shock wave of impact on the coatings results in the effectively coupled thermal-dynamic effects. The HIPIB-irradiated coatings at 3 J/cm^2 and 1 shot still show stable superlattice structure, as well as dense and relatively smooth surface morphology without melting and ablation. However, thermal stress, recoil impulse, stress wave

generation in dynamic process during short duration and termination of pulsed ion beams resulted in the increase of residual stress state, related to slight XRD peak shift to a higher angle. Although the peak shift in XRD patterns is found to have a relationship with residual stress state, chemical composition and crystal structure, it is hard to explore the correlation of slight change in our case with them.

CrN/TiN superlattice coatings deposited by the combined DOMS + PDCMS exhibited high structural stability under HIPIB irradiation up to 3 Jcm^{-2} and 1 shot. Further increasing shot number to 2 times, the superlattice structure with a strong (111) texture disappeared and random orientation feature is detected. Besides, it is clearly seen that the grain coarsening and cracking induced by high stress state are observed on surface morphology of HIPIB-irradiated coatings, leading to the decrease in mechanical properties. The adhesion strength decreases to HF2. However, the irradiated coatings at 1 and 2 shots suffered from severe oxidative and adhesive wear with a lot of wear debris accumulated on sliding wear track, and the partial chipping event is seen on worn surface at 2 shots. In addition, tribocorrosion behavior in seawater reveals the severe plough wear coupled with pitting corrosion due to low surface integrity of irradiated coatings with the formation of microcracks and high surface roughness. When the coating is irradiated at 5 shots, the coatings are detached from substrate. Thus, severe plastic deformation and adhesive wear are occurred owing to the exposed AISI 304L stainless steel during dry sliding wear against 304L balls. Therefore, CrN/TiN superlattice coatings deposited on AISI 304L stainless steel by the combined DOMS + PDCMS exhibit excellent tribological properties in air and seawater under moderate HIPIB irradiation due to high surface integrity and stability of well-defined interfaces and dense microstructure.

5. Conclusions

(1) CrN/TiN superlattice coatings with modulated period of 6.3 nm deposited by the combined deep oscillation magnetron sputtering and pulsed dc magnetron sputtering were irradiated by high-intensity pulsed ion beam (HIPIB) at energy density of 1–3 Jcm^{-2} and shot number of 1–5. The stable superlattice structure with a strong (111)-texture can sustain the impact of shock wave of 3 Jcm^{-2} and 1 shot, while the coatings irradiated at 3 Jcm^{-2} and 2 shots show the random orientation with weak XRD peaks, as well as grain coarsening, surface roughening and even cracking. At 3 Jcm^{-2} and 5 shots, the coatings almost peeled off.

(2) A slight increase of H, E and H/E* and H^3/E^{*2} ratios of HIPIB-irradiated coatings at 1 Jcm^{-2} is obtained with increasing shot number, while the decrease is achieved at 3 Jcm^{-2} and 1–2 shot. The highest H, E and H/E* and H^3/E^{*2} ratios reach 38.7 GPa, 389 GPa, 0.1 and 0.387, respectively. With the increase in energy density from 1 to 3 Jcm^{-2}, the adhesion of coatings irradiated with HIPIB decreases from HF1 to HF6 as the number of shots increases.

(3) At 1 Jcm^{-2} and 1–5 shot, tribological behavior of irradiated coatings in air is dominated by oxidative wear with COF of 0.51 and specific wear rate of 4.2 × 10^{-7}mm^{3}N^{-1}m^{-1}. The irradiated coatings show excellent tribocorrosion properties in seawater with high OCP of 0.32 V, low COF of 0.14 and specific tribocorrosion rate of 6.1 × 10^{-8}mm^{3}N^{-1}m^{-1} without pitting corrosion at under moderate HIPIB irradiation due to high surface integrity and stability of well-defined interfaces and dense microstructure. With an increase of energy density and shot number, wear mechanism in air changes to severe adhesive and oxidative wear, while trobocorrosion mechanism is gradually dominated by plough wear coupled with pitting corrosion.

References

[1] Z.L. Zhang, T. Bell, Structure and corrosion resistance of plasma nitrided stainless steel, Surf. Eng. 1 (1985) 131–136.

[2] J.H. Sung, J.H. Kong, D.K. Yoo, H.Y. On, D.J. Lee, H.W. Lee, Phase changes of the AISI 430 ferritic stainless steels after high-temperature gas nitriding and tempering heat treatment, Mater. Sci. Eng. A 489 (2008) 38–43.

[3] B. Larisch, U. Brusky, H.-J. Spies, Plasma nitriding of stainless steels at low temperatures, Surf. Coat. Technol. 116–119 (1999) 205–211.

[4] E. Carpene, F. Landry, M. Han, K.P. Lieb, P. Schaaf, Investigation of the thermal stability of laser nitrided iron and stainless steel by annealing treatments, Hyperfine Interact. 139 (2002) 355–361.

[5] M.K. Lei, X.M. Zhu, Plasma-based low-energy ion implantation of austenitic stainless steel for improvement in wear and corrosion resistance, Surf. Coat. Technol. 193 (2005) 22–28.

[6] P.Eh Hovsepian, D.B. Lewis, W.-D. Münz, Recent progress in large scale manufacturing of multilayer superlattice hard coatings, Surf. Coat. Technol. 133–134 (2000) 166–175.

[7] Y.X. Ou, H. Chen, Z.Y. Li, J. Lin, W. Pan, M.K. Lei, Microstructure and tribological behavior of TiAlSiN coatings deposited by deep oscillation magnetron sputtering, J. Am. Ceram. Soc. 101 (2018) 5166–5176.

[8] J. Lin, W.D. Sproul, J.J. Moore, S. Lee, Z.L. Wu, R. Chistyakov, B. Abraham, Recent advances in modulated pulsed power magnetron sputtering for surface engineering, JOM 63 (2011) 48–58.

[9] A.S. Kuprin, V.A. Belous, V.N. Voyevodin, V.V. Bryk, R.L. Vasilenko, V.D. Ovcharenko, E.N. Reshetnyak, G.N. Tolmachova, P.N. V'yugov, Vacuum-arc chromium-based coatings for protection of zirconium alloys from the high-temperature oxidation in air, J. Nucl. Mater. 465 (2015) 400–406.

[10] M. Shen, P. Zhao, Y. Gu, S. Zhu, F. Wang, High vacuum arc ion plating NiCrAlY coatings: microstructure and oxidation behavior, Corros. Sci. 94 (2015) 294–304.

[11] J. Paulitsch, P.H. Mayrhofer, W.-D. Münz, M. Schenkel, Structure and mechanical properties of CrN/TiN multilayer coatings prepared by a combined HIPIMS/UBMS deposition technique, Thin Solid Films 517 (2008) 1239–1244.

[12] R. Machunze, A.P. Ehiasarian, F.D. Tichelaar, G.C.A.M. Janssen, Stress and texture in HIPIMS TiN thin films, Thin Solid Films 518 (2009) 1561–1565.

[13] J.C. Oliveira, F. Fernandes, F. Ferreira, A. Cavaleiro, Tailoring the nanostructure of Ti–Si–N thin films by HiPIMS in deep oscillation magnetron sputtering (DOMS) mode, Surf. Coat. Technol. 264 (2015) 140–149.

[14] S. Loquai, O. Zabeida, J.E. Klemberg-Sapieha, L. Martinu, Flash post-discharge emission in a reactive HiPIMS process, Appl. Phys. Lett. 109 (2016) 114101–114106.

[15] J. Lin, B. Wang, Y.X. Ou, W.D. Sproul, I. Dahan, J.J. Moore, Structure and properties of CrSiN nanocomposite coatings deposited by hybrid modulated pulsed power and pulsed dc magnetron sputtering, Surf. Coat. Technol. 216 (2013) 251–258.

[16] Y.X. Ou, J. Lin, S. Tong, H.L. Che, W.D. Sproul, M.K. Lei, Wear and corrosion resistance of CrN/TiN superlattice coatings deposited by a combined deep oscillation magnetron sputtering and pulsed dc magnetron sputtering, Appl. Surf. Sci. 351 (2015) 332–343.

[17] Y.X. Ou, J. Lin, S. Tong, W.D. Sproul, M.K. Lei, Structure, adhesion and corrosion behavior of CrN/TiN superlattice coatings deposited by the combined deep oscillation magnetron sputtering and pulsed dc magnetron sputtering, Surf. Coat.

[18] V.V. Uglov, D.P. Rusalski, S.V. Zlotski, A.V. Sevriuk, G. Abadias, S.B. Kislitsin, K.K. Kadyrzhanov, I.D. Gorlachev, S.N. Du, Stability of Ti-Zr-N coatings under Xe-ion irradiation, Surf. Coat. Technol. 204 (2010) 2095–2098.

[19] A.D. Pogrebnjak, I.V. Yakushchenko, O.V. Bondar, Vyacheslav M. Beresnev, K. Oyoshi, O.M. Ivasishin, H. Amekura, Y. Takeda, M. Opielak, C. Kozak, Irradiation resistance, microstructure and mechanical properties of nanostructured (TiZrHfVNbTa)N coatings, J. Alloy. Comp. 679 (2016) 155–163.

[20] S. Mischler, Triboelectrochemical techniques and interpretation methods in tribocorrosion: a comparative evaluation, Tribol. Int. 41 (2008) 573–583.

[21] Robert J.K. Wood, Tribo-corrosion of coatings: a review, J. Phys. D Appl. Phys. 40 (2007) 5502–5521.

[22] L. Li, L. Liu, X. Li, P. Guo, P. Ke, A. Wang, Enhanced tribocorrosion performance of Cr/GLC multilayered films for marine protective application, ACS Appl. Mater. Interfaces 10 (2018) 13187–13198.

[23] Q. Chen, Y. Cao, Z. Xie, T. Chen, Y. Wan, H. Wang, X. Gao, Y. Chen, Y. Zhou, Y. Guo, Tribocorrosion behaviors of CrN coating in 3.5 wt% NaCl solution, Thin Solid Films 622 (2017) 41–47.

[24] L. Shan, Y. Wang, Y. Zhang, Q. Zhang, Q. Xue, Tribocorrosion behaviors of PVD CrN coated stainless steel in seawater, Wear 362–363 (2016) 97–104.

[25] C. Monticelli, A. Balbo, F. Zucchi, Corrosion and tribocorrosion behaviour of cermet and cermet/nanoscale multilayer CrN/NbN coatings, Surf. Coat. Technol. 204 (2010) 1452–1460.

[26] G.E. Remnev, I.F. Isakov, M.S. Opekounov, V.M. Matvienko, V.A. Ryzhkov, V.K. Struts, I.I. Grushin, A.N. Zakoutayev, A.V. Potyomkin, V.A. Tarbokov, A.N. Pushkaryov, V.L. Kutuzov, M.Yu Ovsyannikov, High intensity pulsed ion beam sources and their industrial applications, Surf. Coat. Technol. 114 (1999) 206–212.

[27] X. Wang, M.K. Lei, J.S. Zhang, Surface modification of 316L stainless steel with high-intensity pulsed ion beams, Surf. Coat. Technol. 201 (2007) 5884–5890.

[28] J. Piekoszewski, J. Langner, High intensity pulsed ion beams in material processing: equipment and applications, Nucl. Instrum. Methods B 53 (1991) 148–160.

[29] X.P. Zhu, Q. Zhang, L. Ding, Z.C. Zhang, N. Yu, A. Pushkarev, M.K. Lei, Deflection of high-intensity pulsed ion beam in focusing magnetically insulated ion diode with a passive anode, Phys. Plasmas 23 (2016) 123101–123108.

[30] J. Pelleg, L.Z. Zevin, S. Lungo, N. Croitour, Reactive-sputter-deposited TiN films on glass substrates, Thin Solid Films 197 (1991) 117–128.

[31] Y.X. Ou, J. Lin, H.L. Che, W.D. Sproul, J.J. Moore, M.K. Lei, Mechanical and tribological properties of CrN/TiN multilayer coatings deposited by pulsed dc magnetron sputtering, Surf. Coat. Technol. 276 (2015) 152–159.

[32] M.K. Lei, X.P. Zhu, C. Liu, J.P. Xin, X.G. Han, P. Li, Z.H. Dong, X. Wang, S.M. Miao, A novel shock processing by high-intensity pulsed ion beam, J. Manuf. Sci. Eng. 131 (2009) 031013–031024.

[33] S.M. Miao, M.K. Lei, Surface morphology of Cr_2O_3 coatings on steel irradiated by high-intensity pulsed ion beam, Nucl. Instrum. Methods B 243 (2006) 335–339.

[34] R. Bayón, A. Igartua, J.J. González, U.R. de Gopegui, Influence of the carbon content on the corrosion and tribocorrosion performance of Ti-DLC coatings for biomedical alloys, Tribol. Int. 88 (2015) 115–125.

[35] S.L. Lehoczky, Strength enhancement in thin-layered Al-Cu laminates, J. Appl. Phys. 49 (1978) 5479–5485.

[36] W. Heinke, A. Leyland, A. Matthews, G. Berg, C. Friedrich, E. Broszeit, Evaluation of PVD nitride coatings, using impact, scratch and Rockwell-C adhesion tests, Thin Solid Films 270 (1995) 431–438.

[37] L. Lutterotti, D. Chateigner, S. Ferrari, J. Ricote, Texture, residual stress and structural analysis of thin films using a combined X-ray analysis, Thin Solid Films 450 (2004) 34–41.

[38] X. Chu, S.A. Barnett, Model of superlattice yield stress and hardness enhancements, J. Appl. Phys. 77 (1995) 4403–4411.